opening of the MC_2B_9 metallacarborane cage has been pointed out[5] as a trend in the structural changes for the isoelectronic 18-electron series $[Re(CO)_3C_2B_9H_{11}]^-$,[12a] $[Au(S_2CNEt_2)C_2B_9H_{11}]$,[11,13c] $[Hg(PPh_3)C_2B_9H_{11}]$,[5,17] and $[TlC_2B_9H_{11}]^-$.[17,18] However, this geometry has been anticipated as a possible structure for $(PPh_3)CuC_2B_9H_{10}(C_5H_5N)$[5] by analogy with the known η^5 structure of $(PPh_3)Cu(C_5H_5)$.[19]

A range of Cu-Cu distances from 2.35 Å to about 3.6 Å is found in polynuclear copper(I) compounds.[20] MO analyses performed with Cu_n^{n+} (n = 2, 4) at the extended Hückel level of approximation supports the existence of a soft and attractive Cu(I)-Cu(I) interaction, overlaid upon the requirements of the bridging ligand set.[20b] In $[Cu_2(tmen)_2(\mu\text{-}CO)(\mu\text{-}PhCO_2)]^+$ the bridging ligand stereochemistry dominates, resulting in the very short Cu(I)-Cu(I) distance of 2.419 (2) Å,[20c] whereas in **3** the stereochemical requirements of the bridging ligand (**1**) are likely to be minimal since the elevation angles of the hydrogen substituents in the $MC_2B_9H_{11}$ cages are not restricted to that of a regular icosahedron.[10b] Thus the relatively close Cu(I)-Cu(I) proximity in **3** can be considered to be a consequence of a metal-metal interaction similar to that found in $Fe_2(CO)_6C_4(CH_3)_2(OH)_2$[21] and its homologues.[22]

Although the isolation of the anionic compound **4** supports the zwitterionic nature of **3**, (PPN)**4** does not convert to **3** in the presence of LCuCl. The dinuclear structural integrity of **3** remains intact upon dissolution although fluxional motions become operative above 253 K since coalescence occurs at this temperature as observed by variable-temperature $^{31}P\{^1H\}$ FTNMR spectroscopy.[8a] At 203 K, the two phosphorus nuclei of **3** are distinguishable while the two CH hydrogens of the carborane cage remain indistinguishable in ^1H NMR, indicating that at least one kind of fluxional motion is still present at this temperature. The evidence at hand does not unequivocally reveal the nature of the fluxional processes.

Acknowledgment. We gratefully acknowledge the support of this work by the Office of Naval Research. We also thank Dr. A. Varadarajan for informative discussions.

Supplementary Material Available: Listings giving the details of the crystallographic data collection, positional and thermal parameters, and interatomic distances and angles (15 pages). Ordering information is given on any current masthead page.

(17) Colquhoun, H. M.; Greenhough, T. J.; Wallbridge, M. G. H. *J. Chem. Soc., Chem. Commun.* **1977**, 737.
(18) Colquhoun, H. M.; Greenhough, T. J.; Wallbridge, M. G. H. *Acta Crystallogr., Sect. B: Struct. Crystallogr. Cryst. Chem.* **1978**, *B34*, 2373.
(19) Cotton, F. A.; Takats, J. *J. Am. Chem. Soc.* **1970**, *92*, 2353.
(20) (a) Reference 3d and references cited therein. (b) Mehrotra, P. K.; Hoffmann, R. *Inorg. Chem.* **1978**, *17*, 2187 and references cited therein. (c) Pasquali, M.; Floriani, C.; Gaetani-Manfredotti, A.; Guastini, C. *J. Am. Chem. Soc.* **1981**, *103*, 185.
(21) Hock, A. A.; Mills, O. S. *Acta Crystallogr.* **1961**, *14*, 139.
(22) (a) Chin, H. B.; Bau, R. *J. Am. Chem. Soc.* **1973**, *95*, 5068. (b) Dettlaf, G.; Weiss, E. *J. Organomet. Chem.* **1976**, *108*, 213.

Department of Chemistry and Biochemistry
University of California, Los Angeles
Los Angeles, California 90024

Youngkyu Do
Han Chyul Kang
Carolyn B. Knobler
M. Frederick Hawthorne*

Received March 5, 1987

Articles

Contribution from the Department of Biology, Faculty of Science, University of Lecce, 73100 Lecce, Italy, and Institute of General and Inorganic Chemistry, University of Parma, 43100 Parma, Italy

Charge Density and Bonding in Bis(dihydrodi-1-pyrazolylborato)nickel(II): $X - X_{HO}$, Multipolar Analysis, and ab Initio Calculation

Dore A. Clemente*[†] and Marina Cingi-Biagini[‡]

Received September 12, 1986

Bis(dihydrodi-1-pyrazolylborato)nickel(II), $[H_2B(C_3N_2H_3)_2]_2Ni^{II}$, crystallized in the orthorhombic space group *Pbca* with a = 17.484 (4) Å, b = 14.534 (3) Å, c = 6.324 (2) Å (room temperature parameters), and Z = 4. The valence electron distribution in this complex has been studied by experimental and theoretical methods. The experimental density distribution was investigated by using two sets of accurate diffraction data collected at 183 and 150 K and analyzed with the atomic multipole technique. Electron density is in excess along the diagonal of the Ni-N directions and along the axis perpendicular to the molecular NiN_4 plane; other deformation density features are observed in the pyrazolyl ring and in the nitrogen lone-pair region. Atomic charge densities (in electrons) are as follows: Ni, +1.06; N(1), -0.32; N(2), -0.26; B, +0.45; C(3), +0.03; C(4), -0.24; C(5), -0.13. Ab initio theoretical calculations are in agreement with the experimental results although atomic charges are predicted to be slightly smaller (in absolute value).

Introduction

Highly accurate, low-temperature, very high angle X-ray diffraction has become a widely used technique to obtain information on the mechanism of bond formation in rather large molecules which are difficult to handle with ab initio methods. Moreover, this technique can supply information on atomic charges and electron densities that is difficult to obtain with other techniques. However, in order to have reliable information, particular attention must be paid to the experimental part: automatic diffractometer, cooling device, and intense-radiation source. These instruments are now generally available, but not everywhere; nevertheless, this is an organization problem and not a scientific one. Moreover, the least-squares refinements with multipole density functions, describing the atomic deformations upon bond formation, produce enhanced Fourier maps virtually free from random noise. The electronic structure of NiN_4 square-planar complexes has been studied extensively not only by theoretical calculations ranging from extended Hückel[1] to CNDO/INDO[2] methods but also by experimental techniques.[3] X-ray diffraction

[†] University of Lecce.
[‡] University of Parma.

(1) Burdett, J. K.; Williams, P. D. *Inorg. Chem.* **1980**, *19*, 2779-2784.
(2) Böhm, M. C. *Theor. Chim. Acta* **1983**, *62*, 373-396.
(3) Nishida, Y.; Kida, S. *Coord. Chem. Rev.* **1979**, *27*, 275-298. See also: Mureinik, R. J. *Rev. Inorg. Chem.* **1979**, *1*, 3-50.

0020-1669/87/1326-2350$01.50/0

Table I. Crystal and Experimental Data

Crystal Data
$[H_2B(C_3N_2H_3)_2]_2Ni^{II}$: M_r = 352.65; space group *Pbca* (D_{2h}^{15}, No. 61); Z = 4
unit cell at room temp:[a,b] a = 17.484 (4), b = 14.534 (3), c = 6.324 (2) Å; V = 1607.01 Å^3
unit cell at 183 K:[a] a = 17.433 (3), b = 14.391 (2), c = 6.228 (1) Å; V = 1562.47 Å^3
unit cell at 150 K:[a] a = 17.498 (3), b = 14.384 (2), c = 6.185 (1) Å; V = 1556.71 Å^3
cryst I: spherical; diameter 0.48 ± 0.02 mm
cryst II: spherical; diameter 0.48 ± 0.02 mm
linear abs coeff: μ = 12.10 cm^{-1} (μR_1 = 0.29, μR_2 = 0.29)
transmission factor: cryst I, 0.6421–0.6516; cryst II, 0.6421–0.6516
weighted path length $\bar{T}$: cryst I, 0.0325–0.0349 cm; cryst II, 0.0325–0.0349 cm
Diffraction Measurements
Collection at 183 K
scanning mode: continuous $\omega/2\theta$
scanning interval in θ: 1.5 + 0.3 tan θ
scanning speed in ω: 2.4° min^{-1}
no. of measmts up to (sin θ)/λ = 0.904 44 Å^{-1} (θ = 40°): 7624
Collection at 150 K
scanning mode: continuous $\omega/2\theta$
scanning interval in θ: 1.6 + 0.3 tan θ
scanning speed in ω: 2.4° min^{-1}
no. of measmts up to (sin θ)/λ = 0.994 94 Å^{-1} (θ = 45°): 9868

[a] Echols and Dennis[10] have described the crystal as *Pbca*, with cell parameters a = 6.331 (2) Å, b = 17.485 (7) Å, and c = 14.519 (3) Å. The matrix P that transforms our results ($a'b'c'$) into those of Echols and Dennis (abc) is ($a'b'c'$) = (abc)[001/100/010]. [b] Dapporto, Mani, and Mealli reported[19] the complex $[H_2B(C_3N_2H_3)_2]_2Cr^{II}$ as *Pbca* with a = 18.076 (5) Å, b = 14.307 (4) Å, and c = 6.130 (3) Å, then in the same orientation as our Ni complex: the two complexes are indeed isostructural; our atomic coordinates are obtained from those of Dapporto et al. by the transformation (x, y, z, → x, $\bar{y}$, $\bar{z}$).

was only rarely used, but good examples are provided by Kutzler et al. for (5,10,15,20-tetramethylporphyrinato)nickel(II)[4] and by Coppens et al. for [*N*,*N*′-bis(2-aminoethyl)malonodiamidato]-nickel(II) trihydrate[5] as well as for iron(II) phthalocyanine,[6] $Co^{II}TPP$[7] (TPP = tetraphenylporpyrin) and $Fe^{III}(OMe)TPP$[8] (OMe = methoxy). We report here a complete experimental electron density and atomic charge density study on the square-planar complex bis(dihydrodi-1-pyrazolylborato)nickel(II), $[H_2B(C_3N_2H_3)_2]_2Ni^{II}$, which is the first noncyclic square-planar Ni complex submitted for multipole analysis.

Experimental Section

A. Sample Preparation and Data Collection. A sample of $[H_2B(C_3N_2H_3)_2]_2Ni^{II}$ was synthesized according to the Trofimenko method[9] and was recrystallized from ethanol as red-orange crystals. The preliminary diffraction experiments showed these crystals are of the same nature as those reported by Echols and Dennis.[10] Some crystals were ground into ellipsoids with the use of the Nonius crystal grinder and were subsequently viewed and manipulated under the microscope and cut into spheres. Two small, almost spherical, samples were selected and their mean radius was measured under a high-magnification microscope. Low-temperature X-ray diffraction intensities were collected for both specimens at two temperatures, 183 and 150 K, on a Philips PW-1100 diffractometer with graphite-monochromated Mo Kα radiation (λ = 0.710 69 Å). The stability of the instrument was monitored by measuring three standard reflections every 60 min. During the first data collection (DC1), carried out at a temperature of 183 K, a total of 7624 reflections were collected up to (sin ϑ)/λ = 0.9044 Å^{-1} (hkl and some $\bar{h}k\bar{l}$ reflections) and no decay of the two spherical specimens was noticed. For improvement of the quality of the data, a second data collection (DC2) was performed at a temperature of 150 K on the same two specimens. Almost two quadrants of reciprocal space were collected up to (sin ϑ)/λ = 0.9949 Å^{-1} (hkl and some $\bar{h}k\bar{l}$ and $\bar{h}kl$), adding up to a total of 9868 measurements. A small amount of decay proportional to the time (4% during data collection, see later) and an increase in the cell parameter a with the lowering in the temperature (see Table I) were observed. A stream of cold nitrogen gas (Leyboldt-Heraeus, NCD1 cooling device) was used for cooling. The temperature of the crystal point was estimated to be ±3 K with a chromel–alumel thermocouple. The cell constants at these temperatures were determined by a least-squares refinement of the setting angles of 25 reflections (Mo Kα_1 radiation, λ = 0.7093 Å; $2\vartheta \simeq$ 50°). The cell parameters at room temperature were determined with essentially the same technique but with 25 reflections of lower 2ϑ values and λ(Mo Kα) = 0.710 69 Å. Other crystallographic and data collection characteristics are summarized in Table I.

B. Data Processing. The distribution of the three standard reflections was analyzed by making a plot of the total integrated intensity of the test reflections vs. time and then the method reported by Lundgren and Liminga for ammonium perchlorate[11] was used. For the first data collection no decrease or variation was observed, while for the second data collection the intensities of the test reflections showed a uniform decrease, following the equation $I_t = I_0(1 - qt)$, with slope q = −0.01089 × 10^{-3} min^{-1}, which was observed when half of the intensities had been collected; after this period the decrease became much more evident and the slope was q = −0.016 00 × 10^{-3} min^{-1} and after 10 days the decrease became further pronounced and we decided to no longer consider the collected reflections.

After the Lorentz and polarization corrections the diffracted intensities were also corrected for absorption by interpolation from calculated tables[12] and the absorption-weighted path lengths were calculated by following the method of ref 13 (program DWIGGI written by R. Wiest at Strasbourg University). The scale factor between the two sets of reflections of crystals I and II was determined by a least-squares procedure in a modified version of the program SORT, which also averages the intensities of all common and crystallographically equivalent reflections, giving an agreement factor (F^2) of 2.2% for DC1 and 2.3% for DC2. The program SORT adds the term p^2I^2 to the variance $\sigma^2(I)$. The fator p, determined from the dispersion of equivalent reflections, turned out to be 0.045 for DC1 and 0.060 for DC2. The variance $\sigma(I)$ was calculated according to

$$\sigma^2(I) = \sigma_c^2(I) + (pI)^2$$

where $\sigma_c(I)$ is the counting variance (Poisson's law) and I is the corrected intensity.

A total of 4876 independent reflections were obtained for DC1, 431 of which had a measured intensity of zero or were negative; only the 3178 independent reflections with $I \geq 3\sigma(I)$ were used for the structure determination. For DC2 the corresponding figures are as follows: 5816 independent reflections, 541 of which with a measured intensity of zero or negative intensity 3802 independent reflections with $I \geq 3\sigma(I)$ used for the structure determination.

C. Least-Squares Refinements. The parameters reported by Echols and Dennis,[10] appropriately adapted to our axis choice (see Table I), were used as a starting set in the least-squares refinements. With the aid of the full-matrix least-squares program LINEX several cycles of refinements were performed on F_0^2 with weights $w = \sigma^{-2}(F_0^2)$. X-ray spherical-atom form factors and anomalous dispersion factors used in the least-squares refinements were taken from ref 14. Isotropic thermal parameters were used, but when R reached a value lower than 0.12, anisotropic temperature factors were introduced for the non-hydrogen atoms. Now, although the positions of the hydrogen atoms were X-ray correct (mean C–H = 0.95 Å), it was noted that their isotropic temperature factors were low; the introduction of the hydrogen form factor of Stewart, Davidson, and Simpson[15] (corresponding to a more contracted atom) resulted in more realistic isotropic thermal parameters for the hydrogen atoms.

(4) Kutzler, F. W.; Swepston, P. N.; Berkovitch-Yellin, Z.; Ellis, D. E.; Ibers, J. A. *J. Am. Chem. Soc.* **1983**, *105*, 2996–3004.
(5) Coppens, P.; Pautler, D.; Griffin, J. F. *J. Am. Chem. Soc.* **1971**, *93*, 1051–1058.
(6) Coppens, P.; Li, L. *J. Chem. Phys.* **1984**, *81*, 1983–1993.
(7) Stevens, E. D. *J. Am. Chem. Soc.* **1981**, *103*, 5087–5095.
(8) Lecomte, C.; Chadwick, D. L.; Coppens, P.; Stevens, E. D. *Inorg. Chem.* **1983**, *22*, 2982–2992.
(9) Trofimenko, S. *J. Am. Chem. Soc.* **1967**, *89*, 3170–3177.
(10) Echols, H. M.; Dennis, D. *Acta Crystallogr., Sect. B: Struct. Crystallogr. Cryst. Chem.* **1976**, *B32*, 1627–1630.
(11) Lundgren, J. O.; Liminga, R, *Acta Crystallogr., Sect. B: Struct. Crystallogr. Cryst. Chem.* **1979**, *B35*, 1023–1027.
(12) Dwiggins, C. W., Jr. *Acta Crystallogr., Sect. A: Cryst. Phys., Diffr., Theor. Gen. Crystallogr.* **1975**, *A31*, 395–396.
(13) Flack, H. D.; Vincent, G. *Acta Crystallogr., Sect. A: Cryst. Phys., Diffr., Theor. Gen. Crystallogr.* **1978**, *A34*, 489–491.
(14) *International Tables for X-ray Crystallography*; Kynoch: Birmingham, England, 1974; Vol. 4, p 99.
(15) Stewart, R. F.; Davidson, E. R.; Simpson, W. T. *J. Chem. Phys.* **1965**, *42*, 3175–3187.

Table II. Details on the Refinement[a] of Structural Data for $[H_2B(C_3N_2H_3)_2]_2Ni^{II}$ at T = 150 K

	conventional refinement[a]	high-order refinement[a]	multipole refinements[b]			
			I	II	III	IV
$(\sin\theta)/\lambda$, Å^{-1}	0.0–1.0	0.7–1.0	0.0–1.0	0.0–1.0	0.0–1.0	0.0–1.0
no. of observns included in refinement	3808	3114	3808	3808	3808	3808
no. of variables	139	106	301	303	223	222
intensity requirements	$I \geq 3\sigma(I)$	none	$I \geq 3\sigma(I)$	$I \geq 3\sigma(I)$	$I \geq 3\sigma(I)$	$I \geq 3\sigma(I)$
$R(F^2)$, %	8.00	6.40	6.27	6.25	6.47	6.43
$R_w(F^2)$, %	10.60	10.70	8.07	8.04	8.31	8.34
$R(F)$, %	4.10	7.40	3.32	3.30	3.41	3.41
$R_w(F)$, %	5.50	6.00	4.16	4.15	4.28	4.30
$10^{-4}g$ (isotropic extinction)	0.22 (4)	0.22 (4)	0.22 (4)	0.22 (4)	0.32 (4)	0.22 (4)
$G = \sum w\Delta^2/(n-m)$	1.402	0.973	1.088	1.084	1.108	1.112
scale factor	4.500	4.389	4.384	4.386	4.406	4.431
constraints	none	none	none	none	yes	yes

[a] All refinements, with inclusion of multipole refinements, were carried out on F^2. In the conventional refinement and in multipole refinement III an isotropic g extinction correction of type I with Lorentzian distribution was carried out. In the high-order refinement the C–H bond distance was fixed at 1.075 Å, while the B–H distance was fixed at 1.20 Å and no refinement on isotropic U parameters was made. The multipole parameters for C and N atoms of pyrazolyl rings containing odd functions of z are constrained to be zero in all multipole refinements. [b] I denotes the multipole refinement without chemical constraints; only the Ni atom was imposed to have a perfect D_{4h} symmetry. The extinction correction was fixed at the value of the full set (0.215×10^4). K and $K'\zeta$ were refined only as a function of atomic species. II denotes refinement as in I, but with the inclusion of two multipole functions (P_{22-} and P_{42-}) for the *mmm* symmetry at the Ni atom site. III denotes refinement as in II, but with constraints deriving from the chemically molecular symmetry $2/m$: N(2)A = N(2)B, N(1)A = N(1)B, C(3)A = C(3)B, C(4)A = C(4)B, H(3)A = H(3)B, H(4)A = H(4)B, and H(5)A = H(5)B with inclusion of isotropic extinction correction as a refinable parameter. IV denotes refinement as in III, but with the isotropic extinction correction fixed at the value of the full set (0.215×10^4).

Table III. Relative Coordinates ($\times 10^5$; $\times 10^4$ for H)

		x	y	z
Ni	*a*	00000	00000	00000
	b	00000	00000	00000
N(1)A	*a*	16106 (5)	−972 (6)	8184 (16)
	b	16103 (6)	−982 (7)	8225 (18)
N(2)A	*a*	9675 (5)	−5814 (6)	2994 (16)
	b	9706 (6)	−5805 (7)	2995 (18)
C(3)A	*a*	11429 (7)	−14908 (8)	4465 (22)
	b	11439 (8)	−14880 (9)	4456 (26)
C(4)A	*a*	19034 (7)	−15951 (8)	10744 (23)
	b	19040 (8)	−15979 (11)	10694 (31)
C(5)A	*a*	21761 (6)	−6956 (8)	12930 (21)
	b	21780 (7)	−6942 (10)	12949 (25)
H(3)A	*a*	770 (10)	−1958 (13)	101 (26)
H(4)A	*a*	2219 (10)	−2181 (12)	1287 (35)
H(5)A	*a*	2665 (10)	−475 (12)	1707 (34)
N(1)B	*a*	9418 (5)	11976 (6)	25476 (16)
	b	9385 (6)	11967 (7)	25475 (18)
N(2)B	*a*	2283 (5)	8307 (6)	22804 (16)
	b	2306 (6)	8327 (8)	22808 (18)
C(3)B	*a*	−1882 (6)	10772 (8)	40091 (20)
	b	−1900 (8)	10773 (9)	40060 (23)
C(4)B	*a*	2542 (7)	16169 (8)	54055 (19)
	b	2537 (9)	16163 (10)	54068 (21)
C(5)C	*a*	9644 (7)	16691 (8)	44167 (19)
	b	9657 (8)	16707 (9)	44135 (22)
H(3)B	*a*	−705 (10)	857 (12)	4124 (34)
H(4)B	*a*	76 (9)	1865 (13)	6867 (36)
H(5)B	*a*	1403 (12)	2001 (12)	4761 (30)
B	*a*	15791 (7)	9771 (9)	8787 (22)
	b	15790 (9)	9782 (10)	8774 (25)
H(1)	*a*	2122 (9)	1262 (12)	1467 (32)
H(2)	*a*	1353 (10)	1249 (11)	−773 (33)

[a] From conventional refinement of the full set of X-ray data, with the condition $I_{obsd} > 3\sigma(I_{obsd})$. [b] From high-order refinement $(\sin\theta)/\lambda > 0.70$ Å^{-1}, with all reflections included.

Secondary isotropic extinction dominated by mosaic spread (type I) with a Lorentzian distribution function was assumed, and the corresponding parameter g was refined, according to the method of Becker and Coppens.[16] The final value of g was 0.22 (4) $\times 10^4$; the mosaic spread was 12 in. At this point a careful examination of F_o and F_c tables showed that the reflections more affected by extinction were 002 (y =0.85), 020 (y = 0.72), 111 (y = 0.84), 131 (y = 0.85), and 200 (y = 0.69). Since on reflection, 002, was overcorrected, while 020 and 200 were still undercorrected, we attempted some anisotropic extinction corrections with the method of Hamilton and Coppens[17] and with the method of Nelmes and Thornley,[18] but ultimately no improvement was obtained with these anisotropic methods.

In the next step, a high-angle refinement was performed with the use of all the 3114 reflections with $\vartheta > 30°$ (i.e. $(\sin\vartheta)/\lambda > 0.70$ Å^{-1}) without any conditions on the intensity. The C–H distance was fixed at 1.075 Å in the geometrical positions; the B–H distance was imposed at 1.20 Å always in the geometrical position. R,R_w, and other agreement factors are reported in Table II. The "goodness of fit" $G = [\sum w\Delta^2/(n-m)]^{1/2}$ (n = number of reflections, m = least-squares variables, $\Delta = F_o - F_c$) is very near to 1 for the high-order data as the theory requires. The positional parameters obtained from the refinement of the full and

Table IV. Bond Lengths (Å) and Angles (deg) in $[H_2B(C_3N_2H_3)_2]_2Ni^{II}$ at 150 K

	ring A		ring B	
	a	*b*	*a*	*b*
Ni–N(2)	1.897 (1)	1.902 (1)	1.891 (1)	1.894 (1)
N(1)–N(2)	1.362 (1)	1.356 (2)	1.366 (1)	1.355 (2)
N(2)–C(3)	1.347 (2)	1.343 (2)	1.342 (2)	1.343 (2)
N(1)–C(5)	1.344 (1)	1.344 (2)	1.341 (2)	1.341 (2)
C(3)–C(4)	1.394 (2)	1.394 (2)	1.396 (2)	1.398 (2)
C(4)–C(5)	1.386 (2)	1.393 (2)	1.387 (2)	1.391 (2)
C(3)–H(3)	0.96 (2)		0.96 (2)	
C(4)–H(4)	1.02 (2)		1.02 (2)	
C(5)–H(5)	0.95 (2)		0.93 (2)	
N(1)–B	1.547 (2)		1.552 (2)	
B–H(1)	1.10 (2)			
B–H(2)			1.16 (2)	
N(2)–N(1)–C(5)	109.41 (9)	109.61 (11)	109.07 (9)	109.49 (11)
N(1)–C(5)–C(4)	108.85 (10)	108.61 (12)	109.05 (10)	108.64 (12)
C(5)–C(4)–C(3)	104.80 (11)	104.50 (12)	104.73 (10)	104.76 (12)
C(3)–N(2)–N(1)	107.01 (9)	107.14 (10)	107.34 (9)	107.64 (11)
N(2)–N(1)–B	119.16 (9)	119.16 (10)	119.83 (9)	119.97 (11)
H(3)–C(3)–N(2)	120.6 (1.0)		118.9 (1.2)	
H(3)–C(3)–C(4)	129.4 (1.1)		131.3 (1.2)	
H(4)–C(4)–C(3)	130.1 (1.0)		125.0 (0.9)	
H(4)–C(4)–C(5)	125.1 (1.0)		130.2 (1.0)	
H(5)–C(5)–N(1)	120.6 (1.1)		118.8 (1.2)	
H(5)–C(5)–C(4)	130.5 (1.1)		131.8 (1.1)	
N(2)A–Ni–N(2)B	90.99 (4)			
H(1)–B–H(2)	117.41 (1.30)			
N(1)A–B–N(1)B	104.23 (9)			

[a] Full-set coordinates. [b] High-order coordinates.

(16) Becker, P.; Coppens, P. *Acta Crystallogr., Sect. A: Cryst. Phys., Diffr., Theor. Gen. Crystallogr.* **1975**, *A31*, 417–425.

(17) Coppens, P.; Hamilton, W. C. *Acta Crystallogr., Sect. A: Cryst. Phys., Diffr., Theor. Gen. Crystallogr.* **1970**, *A26*, 71–83.

(18) Thornley, F. R.; Nelmes, R. J. *Acta Crystallogr., Sect. A: Cryst. Phys., Diffr., Theor. Gen. Crystallogr.* **1974**, *A30*, 748–757.

Table V. Equations of Planes, Angles between Planes (deg), and Displacement of Atoms from Planes (Å × 10^3)[a,b] at 150 K

plane A	coordination square plane: Ni, N(2)A, N(2)B $[-0.3887\ (6)]X - [0.6445\ (5)]Y + [0.6584\ (4)]Z = 0.0000$
plane B	ring A: N(1) (1), N(2) (0), C(3) (0), C(4) (1), C(5) (−1), Ni (−298),* B(−50)* $[0.2793\ (7)]X - [0.0017\ (8)]Y - [0.9602(2)]Z = 0.2982\ (21)$
plane C	ring B: N(1) (−1), N(2) (2), C(3) (−3), C(4) (2), C(5) (0), Ni (−201),* B (−93)* $[-0.2894\ (7)]X + [0.8296\ (4)]Y - [0.4775\ (6)]Z = 0.2013\ (21)$
plane D	Ni, B, H(1), H(2) $[0.4732\ (5)]X - [0.7528\ (8)]Y - [0.4576\ (15)]Z = 0.0000$ N(2)A (1347),* N(1)A (1207),* C(3)A (2432),* C(4)A (3004),* C(5)A (2189)* N(2)B (−1356), N(1)B (−1240),* C(3)B (−2458),* C(4)B (−3070),* C(5)B (−2258)
dihedral angles	A–B = 137.70 (6), A–C = 137.45 (5), B–C = 67.89 (5), A–D = 90.00

[a] Equations of planes are in the form $AX + BY + CZ = D$, where X, Y, and Z are the coordinates in Å referred to orthogonal axes and obtained from the fractional ones by applying the matrix [a00/0b0/00c]. Atom displacements are given in parentheses. [b] Asterisks mark atoms not included in the plane calculation.

high-order data are given in Table III. Anisotropic thermal parameters U_{ij} from high-order refinement and isotropic thermal parameters for hydrogen atoms are available (see the supplementary material). The bond lengths and angles are reported in Table IV, while least-squares planes and distances from the plane are listed in Table V. Comparison of the conventional results with high-angle refinement results indicates that the asphericity shifits are in the order N(1)B (0.0059 Å), N(2)A (0.0056 Å), C(4)A (0.0052 Å), N(2)B (0.0050 Å), etc.; although they are quite small (less than 0.01 Å), they clearly indicate the electronic situation. For example the Ni–N(2) bond distances in the conventional refinement are shorter, since the N(2) atoms are shifted toward the Ni atom to partially compensate the electron density of the N lone pair.

Results and Discussion

A. Molecular Geometry and Dimensions. Since an accurate description of the molecular geometry has been already given by Echols and Dennis,[10] here we discuss only the aspects that are made clearer by the more accurate bond distances we obtained: they show now a better agreement between the two pyrazolyl rings, especially with high-angle data ($\sum|\Delta|$ = 0.015 Å (full set) 0.010 Å high order)). In fact we want to emphasize the presence of a molecular (noncrystallographic) mirror plane passing through the Ni, B, H(1), and H(2) atoms and bisecting the two pyrazolyl rings. This molecular mirror plane (C_s) and the crystallographic center of symmetry impose on the whole molecule a $2/m$ point group, with the binary axis contained in the equatorial plane. Moreover, we find in the molecule a small amount of asymmetry, which is evident in the two Ni–N(2)A = 1.902 (1) Å and Ni–N(2)B = 1.894 (1) Å distances and in the different displacements of the Ni atom from the two pyrazolyl rings, the highest displacement (0.298 Å) corresponding to the longest Ni–N distance (1.902 Å), thus indicating that the difference is real. To reduce the N(2)A–Ni–N(2)B coordination angle, here 90.99 (4)°, to 90.00°, as a regular square-planar coordination requires, the pyrazolyl ligand reduces the N(1)A–B–N(1)B angle to 104.23 (9)° against the 109.5° tetrahedral value or the 106.64° value found in $[H_2B(C_3N_2H_3)_2]_2Cr^{II}$,[19] the 109.8–115.6° range found in $K\{[H_2B(C_3N_2H_3)_2]_3V\}$[19] or the 107.51 (7)° value in $[Ph_2B(Pz)_2][\eta^3\text{-}CH_2CH(CH_3)CH_2](CO)_2Mo$.[20] However, the angle contraction is not sufficient and the Ni atom is still out of the planes of the pyrazolyl rings (Table V).

B. Electron Density Maps. The $X - X_{HO}$ deformation density $\rho_{X-X}(\mathbf{r})$ was calculated. This is defined in real space as

$$\rho_{X-X}(\mathbf{r}) = \rho_{cryst}(\mathbf{r}) - \sum\rho_{free\ atom} = \rho_{obsd}(\mathbf{r})/K - \rho_{calcd}(\mathbf{r})$$

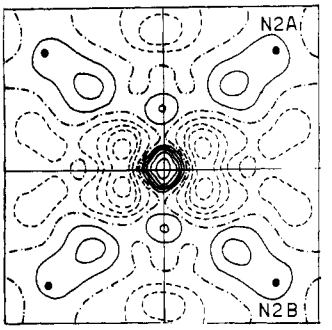

Figure 1. Observed deformation electron density ($X - X_{HO}$) in the square NiN_4 plane after averaging over chemically equivalent atoms, i.e. imposition of the *mmm* molecular symmetry on the square-planar NiN_4 group. The mirror planes are indicated. Contours are at 0.1 e Å^{-3} intervals. The DC1 data set used, $[(\sin\theta)/\lambda]_{max} \leq 0.90$ Å^{-1}; all reflections with $I \geq 3\sigma(I)$ were included (temperature 183 K). Dashed contours are for negative and bold lines for zero deformation electron density.

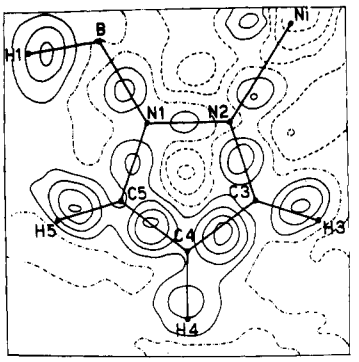

Figure 2. Observed deformation electron density ($X - X_{HO}$) averaged over the two pyrazolyl rings A and B. The DC1 data set was used, with $[(\sin\theta)/\lambda]_{max} \leq 0.60$ Å^{-1}; all reflections with $I \geq 3\sigma(I)$ were included. Contours are as in Figure 1 (temperature 183 K).

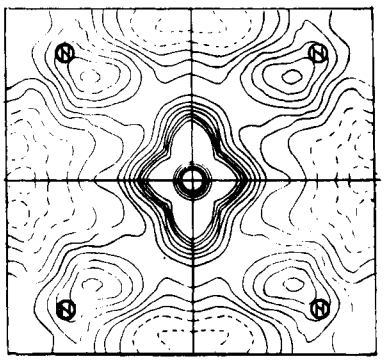

Figure 3. Observed deformation electron density in the square NiN_4 plane after averaging over chemically equivalent atoms, i.e., imposition of the *mmm* molecular symmetry on the square-planar NiN_4 group. The mirror planes are indicated. Contours are at 0.1 e Å^{-3} intervals. The DC2 data set was used, with $[(\sin\theta)/\lambda]_{max} \leq 1.00$ Å^{-1}; all reflections with $I \geq 3\sigma(I)$ were included (temperature 150 K).

where $\rho_{obsd}(\mathbf{r})$ is the Fourier transform of the unscaled observed structure factor, corrected for anomalous dispersion effects, or more operatively in reciprocal space

$$\rho_{X-X}(\mathbf{r}) = \frac{2}{V}\sum_{0}^{H}(F_o - F_c(\text{high order}))\exp(2\pi i\mathbf{h}\cdot\mathbf{r})$$

where the calculated amplitudes are based on parameters from high-order refinement and spherical atom scattering factors and the sign of F_c is assigned to F_o. The $X - X$ maps have an advantage over the conventional difference maps because the aspherical features in the atomic electron density are more pronounced since the F_c values are calculated with high-order parameters, which are much less biased by the aspherical features.

Some deformation densities through the equatorial plane or though the pyrazolyl rings A and B are reported in Figures 1–9.

(19) Dapporto, P.; Mani, F.; Mealli, C. *Inorg. Chem.* **1978**, *17*, 1323–1329.
(20) Cotton, F. A.; Frenz, B. A.; Murillo, C. A. *J. Am. Chem. Soc.* **1975**, *97*, 2118–2122.

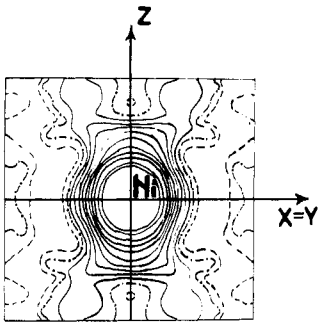

Figure 4. Observed deformation electron density ($X - X_{HO}$) plotted through a plane that is perpendicular to the NiN_4 square plane and passes midway between the N(2)A and N(2)B atoms. Contours and other details are as in Figure 3.

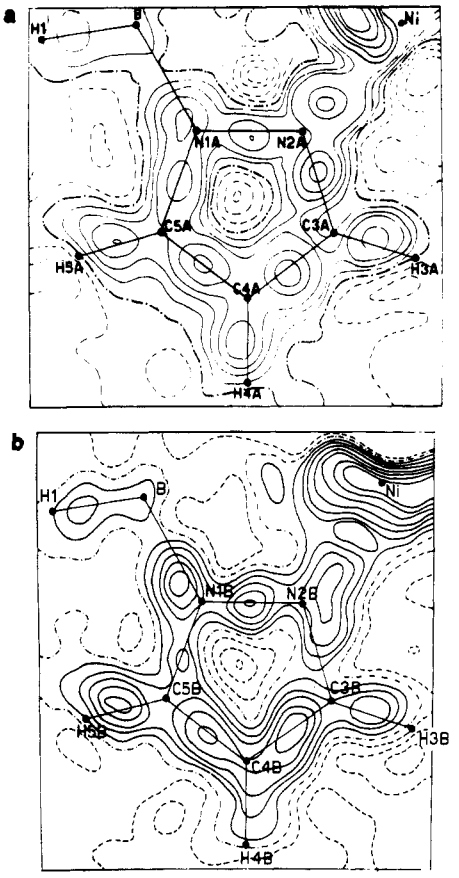

Figure 5. Observed deformation electron density ($X - X_{HO}$) plotted through (a) pyrazolyl ring A and (b) pyrazolyl ring B. $[(\sin\theta)/\lambda]_{max} \leq 0.70$ Å^{-1}; all reflections with $I \geq 3\sigma(I)$ were included. Contours and other details are as in Figure 3.

Most of the density maps reproduced here are from the study at 150 K (DC2); although bonding electrons are clearly visible also at $T = 183$ K, the maps at lower temperature ($T = 150$ K) are of superior quality especially for the pyrazolyl rings.

Electron density maps show prominent peaks corresponding to electron accumulation in the middle of the bonds. A maximum shifted toward the nitrogen atoms (at $\simeq$0.5 Å) and interpreted as the N lone pair (height of ca. 0.5 e/Å^3) is present in the Ni–N bonds; also the N–B bonds show a maximum shifted toward the more electronegative nitrogen atoms, and this could be related to the high positive charge exhibited by the B atom. The peaks are in the order C–C > C–N $\simeq$ N–N > C–H > N–B; the two rings show a chemical symmetry also in this regard. Moreover, in the maps no indication is present of alternating single-bond–double-bond character distributed over the ring. These bond distances and electron density maxima strongly suggest that electron delocalization extends over the five-membered ring.

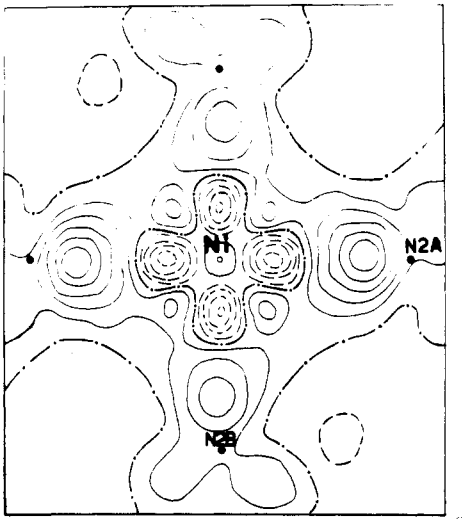

Figure 6. Model deformation electron density (aspherical model density minus spherical model density) after multipole refinement I, plotted on the NiN_4 square plane. Contours and other details are as in Figure 3.

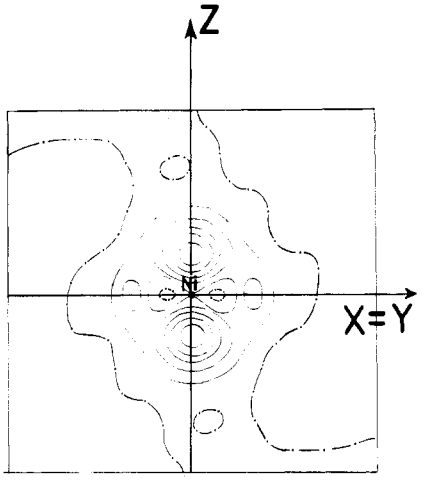

Figure 7. Model deformation electron density (aspherical model density minus spherical model density) after multipole refinement I, plotted through a plane that is perpendicular to the NiN_4 square plane and passes midway between the N(2)A and N(2)B atoms. Contours and other details are as in Figure 3.

The area around the Ni atom is important for assessing the bonding situation of the metal atom. In the equatorial plane it shows density accumulation relative to the spherical Ni atom, along the xy diagonal, indicating more average occupancy of the d_{xy} orbital. The electron density at the Ni site is higher than expected, but this is not surprising and is principally due to the scaling errors in scale factor K as explained by Rees.[21] Therefore, to limit these errors, the scale factor K is determined by a least-squares refinement in which positional and thermal parameters are fixed at their high-angle values. However, this technique was also not completely successful and the maps in Figures 1 and 3 still show a high electron density at the Ni site, especially for the map at 150 K. Much of the difference between Figures 1 and 3 comes from this phenomenon, but the chemical significance of the two maps is similar, both indicating an electron accumulation along the xy diagonal.

More detailed maps will be presented in the following section, where multipole refinement is applied.

C. Multipole Refinements and Maps. The multipole refinement technique was introduced in the analysis of X-ray diffraction data by several authors, especially De Marco and Weiss, Dawson, Stewart, Hirshfeld, and, most of all, Coppens et al.[22] for describing

(21) Rees, B. *Acta Crystallogr., Sect. A: Cryst. Phys., Diffr., Theor. Gen. Crystallogr.* **1976**, *A32*, 483–488.

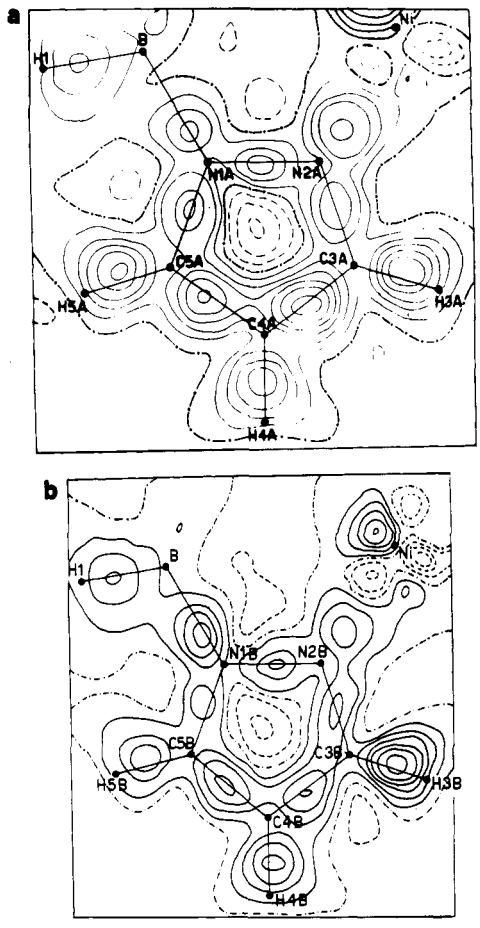

Figure 8. Model deformation electron density (aspherical model density minus spherical model density) after multipole refinement I, calculated through (a) pyrazolyl ring A and (b) pyrazolyl ring B. Contours and other details are as in Figure 3.

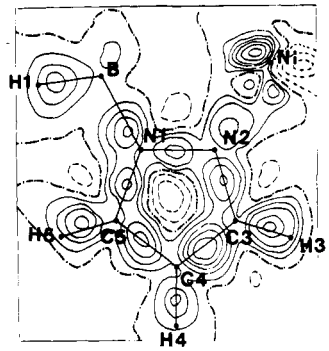

Figure 9. Model deformation electron density (aspherical model density minus spherical model density) after multipole analysis with deformation parameters of ring A constrained to be equal to those of ring B, i.e., with $2/m$ symmetry imposed for the whole molecule. Contours and other details are as in Figure 3.

the atomic deformation upon formation of chemical bonds.

Each atomic density is now divided in a core part identical with the core density of the free atom and a valence part flexible enough to reflect the chemical deformation

$$\rho_{atom}(r) = \rho_{core}(r) + P_v K^3 \rho_v(Kr) + \sum_{l=0}^{4} R_l(K'r) \sum_{m=-l}^{l} P_{lm} K'^3 y_{lm}(\mathbf{r}/r)$$

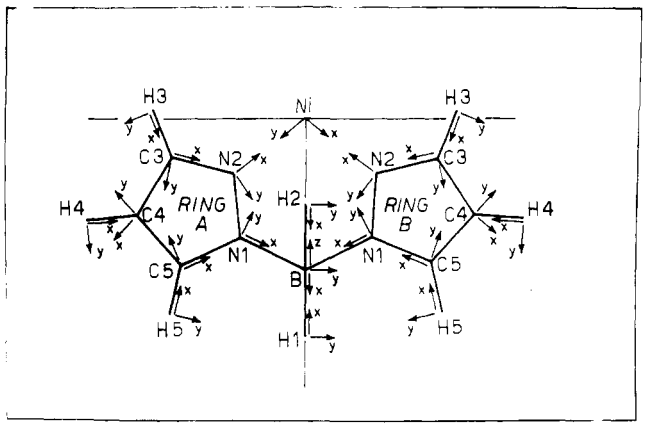

Figure 10. Local coordinate systems (one for each atom) used in the multipole refinement. Note that the systems reflect the $2/m$ molecular symmetry of the whole molecule (see text): with these symmetry constraints multipole refinements III and IV were carried out.

where y_{lm} represents spherical harmonic angular functions in real form, defined relative to local atomic coordinate systems, one for each atom, as reported in Figure 10. P_v and P_{lm} are population coefficients of valence and multipole basis functions and are refinable parameters as are the expansion–contraction parameters K and K'; $R_l(r)$ is the radial part of these "multipole" functions

$$R_l(r) = Nr^{nl} \exp(-\zeta r)$$

where N is a normalization factor and n_l and ζ are chosen for each l value; the choice of the exponent n_l was made by following the results of Coppens.[22] The n_l values used are as follows: for Ni 4, 4, 4, and 4 and for B, C, and N 2, 2, 3, and 4 for l = 1, 2, 3, and 4, respectively; for hydrogen n_l = 1 for l = 1.

Because of the large number of parameters to be optimized (26 for each atom), we have imposed a number of constraints on the population parameters due to local symmetry: First, in all refinements the P_{10}, P_{21+}, P_{21-}, etc. multipole parameters for the atoms of rings A and B containing an odd function of z were constrained to be zero and a mirror plane coinciding with the pyrazolyl ring was assumed. Second, the symmetry at Ni was imposed to be D_{4h}, so reducing the population parameters to P_{20}, P_{40}, and P_{44+}, or to D_{2h} (the true molecular symmetry at the Ni site) thus adding P_{22-} and P_{42-} to the refinable population parameters. Usually in D_{2h} = mmm symmetry the allowed multipole functions are y_{22+} $[(x^2 - y^2)]$ and y_{42+} $[(x^2 - y^2), ...]$ since the coordinate axes x, y, z are chosen to be coincident with the two fold axes. However, in our case the x, y axes are situated at 45° between the two fold axes (Figure 10); thus, y_{22-} $[(xy)]$ and y_{42-} [(xy), ...] are the allowed multipole functions.

The population parameters at B containing an odd function of y were disregarded for the presence of the molecular mirror C_s passing through Ni, B, H(1), and H(2). The deformation of the H atoms was described by a single dipole along the C–H axis. Therefore, each local atomic coordinate system was defined by taking into account the molecular mirror plane C_s; it was thus possible to carry out more constrained refinements (III and IV) in which the populations of chemically equivalent atoms have been constrained to be equal, reducing the refinable parameters again.

Furthermore, some multipole refinements were carried out with the extinction factor g fixed at the value of the conventional refinement and others with g as a refinable parameter; also, some anisotropic extinction refinements were carried out. It was found that the inclusion of g or g_{ij} in the multipole refinement did not give any significant improvement in R factors and generally raises the atomic charge at Ni, N(2), N(1), and especially B, and so it is not advisable to insert the refinement of extinction parameters during multipole analyses for our crystals affected by extinction corrections; thus, we have used the excitation parameter fixed at the value of the conventional refinement.

(22) (a) Hansen, N. K.; Coppens, P. *Acta Crystallogr., Sect. A: Cryst. Phys., Diffr., Theor. Gen. Crystallogr.* **1978**, *A34*, 909–921. (b) Baert, F.; Coppens, P.; Stevens, E. D. *Acta Crystallogr., Sect. A: Cryst. Phys., Diffr., Theor. Gen. Crystallogr.* **1982**, *A38*, 143–151. (c) Holladay, A.; Leung, P.; Coppens, P. *Acta Crystallogr., Sect. A: Found. Crystallogr.* **1983**, *A39*, 377–387.

(23) Reference deleted in revision.

Table VI. Multipole Populations at 150 K

	refinement			
	I	II	III	IV
Ni				
K	0.98 (1)	0.97 (1)	0.96 (1)	0.97 (1)
$K'\zeta$	5.76 (8)	6.07 (8)	6.08 (8)	6.00 (8)
P_v	9.28 (11)	9.30 (11)	9.58 (11)	8.95 (9)
P_{20}	0.25 (2)	0.25 (2)	0.26 (2)	0.26 (2)
P_{22-}		−0.08 (2)	−0.07 (2)	−0.06 (2)
P_{40}	0.05 (2)	0.05 (2)	0.02 (2)	0.02 (2)
P_{42-}		0.15 (2)	0.15 (2)	0.15 (2)
P_{44+}	−0.22 (1)	−0.22 (1)	−0.22 (1)	−0.22 (1)
N(2)A				
K	1.00 (1)	1.00 (1)	1.00 (1)	1.00 (1)
$K'\zeta$	3.06 (4)	3.13 (4)	2.95 (4)	2.99 (5)
P_v	5.38 (13)	5.36 (12)	5.38 (11)	5.26 (9)
P_{11+}	0.13 (5)	0.12 (5)	0.14 (4)	0.13 (3)
P_{11-}	−0.13 (6)	−0.12 (5)	−0.05 (5)	−0.07 (3)
P_{20}	−0.25 (4)	−0.24 (4)	−0.18 (3)	−0.18 (3)
P_{22+}	0.18 (4)	0.17 (4)	0.11 (3)	0.11 (3)
P_{22-}	0.09 (5)	0.09 (4)	0.05 (4)	0.05 (3)
P_{31+}	0.01 (6)	0.01 (3)	−0.02 (3)	−0.01 (2)
P_{31-}	−0.05 (4)	−0.05 (4)	−0.05 (3)	−0.05 (3)
P_{33+}	0.18 (4)	0.17 (4)	0.21 (4)	0.20 (3)
P_{33-}	0.05 (5)	0.04 (4)	0.02 (4)	0.03 (3)
P_{40}	−0.12 (5)	−0.11 (4)	0.04 (3)	0.05 (3)
P_{42+}	−0.06 (5)	−0.05 (4)	−0.13 (4)	−0.12 (3)
P_{42-}	0.13 (5)	0.13 (4)	0.07 (4)	0.07 (3)
P_{44+}	−0.03 (5)	−0.04 (4)	0.02 (4)	0.03 (3)
P_{44-}	−0.01 (5)	0.00 (4)	0.01 (4)	0.01 (3)
N(1)A				
K	1.00 (1)	1.00 (1)	1.00 (1)	1.00 (1)
$K'\zeta$	3.06 (4)	3.13 (4)	2.95 (4)	2.99 (5)
P_v	5.43 (14)	5.40 (14)	5.48 (12)	5.32 (1)
P_{11+}	0.09 (6)	0.08 (5)	0.10 (5)	0.10 (4)
P_{11-}	0.06 (6)	0.05 (5)	0.01 (5)	0.01 (4)
P_{20}	−0.20 (5)	−0.20 (4)	−0.18 (3)	−0.16 (3)
P_{22+}	0.02 (5)	0.01 (4)	0.07 (4)	0.06 (3)
P_{22-}	0.01 (5)	0.00 (4)	−0.06 (4)	−0.07 (3)
P_{31+}	0.06 (4)	0.05 (3)	0.03 (3)	0.03 (3)
P_{31-}	0.04 (5)	0.03 (4)	−0.02 (3)	−0.03 (3)
P_{33+}	0.28 (5)	0.25 (4)	0.27 (4)	0.25 (4)
P_{33-}	0.02 (5)	0.02 (4)	0.01 (4)	0.00 (3)
P_{40}	−0.15 (6)	−0.13 (5)	0.00 (4)	0.00 (3)
P_{42+}	0.25 (6)	0.24 (5)	0.23 (4)	0.21 (4)
P_{42-}	0.02 (5)	0.02 (4)	−0.01 (4)	−0.02 (3)
P_{44+}	−0.16 (6)	−0.15 (5)	−0.13 (5)	−0.14 (4)
P_{44-}	0.14 (5)	0.13 (4)	0.11 (4)	0.12 (3)
C(3)A				
K	1.03 (1)	1.02 (1)	1.02 (1)	1.01 (1)
$K'\zeta$	2.45 (2)	2.44 (2)	2.49 (2)	2.61 (3)
P_v	3.82 (17)	3.81 (16)	3.84 (14)	3.97 (12)
P_{11+}	−0.03 (9)	−0.02 (8)	0.01 (7)	−0.01 (5)
P_{11-}	−0.18 (7)	−0.19 (9)	−0.03 (7)	−0.05 (5)
P_{20}	−0.40 (6)	−0.39 (6)	−0.37 (4)	−0.33 (4)
P_{22+}	−0.08 (7)	−0.08 (7)	−0.11 (5)	−0.10 (4)
P_{22-}	0.13 (7)	0.13 (7)	0.13 (5)	0.14 (4)
P_{31+}	0.00 (6)	0.00 (6)	−0.05 (4)	−0.05 (3)
P_{31-}	0.09 (6)	0.09 (6)	0.06 (4)	0.04 (4)
P_{33+}	0.46 (8)	0.46 (8)	0.56 (6)	0.46 (5)
P_{33-}	−0.06 (8)	−0.07 (7)	−0.06 (6)	−0.04 (4)
P_{40}	0.06 (7)	0.06 (7)	0.11 (5)	0.10 (4)
P_{42+}	0.13 (7)	0.14 (7)	0.12 (5)	0.11 (4)
P_{42-}	−0.08 (7)	−0.08 (7)	0.00 (5)	−0.01 (4)
P_{44+}	−0.09 (8)	−0.09 (8)	−0.03 (5)	0.02 (4)
P_{44-}	−0.27 (8)	−0.29 (8)	−0.14 (6)	−0.15 (5)
C(4)A				
K	1.03 (1)	1.02 (1)	1.02 (1)	1.01 (1)
$K'\zeta$	2.45 (2)	2.44 (2)	2.49 (2)	2.61 (3)
P_v	4.29 (20)	4.30 (19)	4.15 (15)	4.24 (12)
P_{11+}	−0.14 (10)	−0.14 (9)	0.01 (7)	−0.04 (5)
P_{11-}	0.17 (11)	0.17 (9)	0.07 (7)	0.06 (6)
P_{20}	−0.41 (7)	−0.42 (7)	−0.36 (5)	−0.30 (4)
P_{22+}	0.31 (8)	0.32 (8)	0.13 (6)	0.09 (5)
P_{22-}	−0.03 (8)	−0.02 (7)	0.00 (5)	−0.06 (4)
P_{31+}	−0.07 (7)	−0.06 (7)	−0.10 (5)	−0.06 (4)
P_{31-}	−0.03 (8)	−0.03 (7)	−0.08 (5)	−0.04 (4)
P_{33+}	−0.34 (9)	−0.34 (9)	−0.31 (6)	−0.24 (5)
P_{33-}	−0.38 (8)	−0.39 (8)	−0.39 (6)	−0.34 (5)
P_{40}	−0.03 (8)	−0.03 (7)	0.04 (5)	0.00 (4)
P_{42+}	−0.09 (8)	−0.09 (8)	−0.06 (5)	0.00 (4)
P_{42-}	0.33 (8)	0.33 (8)	0.20 (5)	0.21 (5)
P_{44+}	0.05 (8)	0.04 (8)	0.02 (6)	0.04 (5)
P_{44-}	0.06 (9)	0.05 (9)	0.14 (6)	0.06 (5)
C(5)A				
K	1.03 (1)	1.02 (1)	1.02 (1)	1.01 (1)
$K'\zeta$	2.45 (2)	2.44 (2)	2.49 (2)	2.61 (3)
P_v	4.02 (18)	4.00 (16)	4.15 (15)	4.13 (12)
P_{11+}	0.04 (9)	0.06 (9)	0.08 (7)	0.07 (5)
P_{11-}	0.19 (9)	0.19 (9)	0.12 (7)	0.08 (5)
P_{20}	−0.48 (7)	−0.48 (7)	−0.33 (5)	−0.28 (4)
P_{22+}	−0.21 (8)	−0.20 (7)	−0.21 (6)	−0.15 (4)
P_{22-}	0.12 (7)	0.10 (7)	0.12 (5)	0.07 (4)
P_{31+}	−0.10 (7)	−0.12 (7)	−0.08 (5)	−0.10 (3)
P_{31-}	0.10 (7)	0.10 (7)	0.08 (5)	0.05 (4)
P_{33+}	0.46 (9)	0.47 (8)	0.42 (6)	0.36 (5)
P_{33-}	0.05 (8)	0.04 (8)	0.09 (6)	0.06 (5)
P_{40}	−0.02 (7)	−0.01 (7)	0.04 (5)	0.05 (4)
P_{42+}	0.03 (8)	0.01 (7)	0.01 (5)	−0.02 (4)
P_{42-}	−0.32 (9)	−0.32 (8)	−0.22 (5)	−0.19 (4)
P_{44+}	0.18 (9)	0.19 (9)	0.21 (6)	0.21 (5)
P_{44-}	−0.11 (8)	−0.09 (8)	−0.18 (6)	−0.13 (5)
N(2)B				
K	1.00 (1)	1.00 (1)		
$K'\zeta$	3.06 (4)	3.13 (4)		
P_v	5.47 (13)	5.45 (12)		
P_{11+}	0.05 (5)	0.06 (5)		
P_{11-}	−0.03 (6)	−0.02 (5)		
P_{20}	−0.14 (4)	−0.14 (4)		
P_{22+}	0.04 (5)	0.02 (4)		
P_{22-}	−0.01 (5)	−0.02 (4)		
P_{31+}	−0.05 (3)	−0.04 (3)		
P_{31-}	−0.04 (4)	−0.04 (4)		
P_{33+}	0.21 (5)	0.21 (4)		
P_{33-}	−0.02 (5)	−0.01 (4)		
P_{40}	0.23 (5)	0.24 (5)		
P_{42+}	−0.21 (5)	−0.19 (4)		
P_{42-}	0.04 (7)	0.04 (4)		
P_{44+}	0.00 (5)	0.01 (5)		
P_{44-}	−0.05 (5)	−0.02 (5)		
N(1)B				
K	1.00 (1)	1.00 (1)		
$K'\zeta$	3.06 (4)	3.13 (4)		
P_v	5.34 (14)	5.30 (13)		
P_{11+}	0.14 (6)	0.12 (5)		
P_{11-}	0.06 (6)	0.04 (5)		
P_{20}	−0.09 (4)	−0.08 (4)		
P_{22+}	0.11 (5)	0.10 (4)		
P_{22-}	−0.08 (5)	−0.07 (4)		
P_{31+}	0.00 (4)	−0.01 (3)		
P_{31-}	−0.02 (4)	−0.02 (3)		
P_{33+}	0.25 (5)	0.24 (4)		
P_{33-}	0.03 (5)	0.02 (4)		
P_{40}	0.07 (5)	0.06 (4)		
P_{42+}	0.17 (5)	0.15 (4)		
P_{42-}	−0.07 (5)	−0.07 (4)		
P_{44+}	−0.01 (6)	−0.04 (5)		
P_{44-}	0.12 (6)	0.11 (5)		
C(3)B				
K	1.03 (1)	1.02 (1)		
$K'\zeta$	2.45 (2)	2.44 (2)		
P_v	3.96 (18)	4.00 (18)		
P_{11+}	−0.03 (10)	−0.03 (9)		
P_{11-}	−0.06 (10)	−0.05 (9)		
P_{20}	−0.21 (6)	−0.22 (6)		
P_{22+}	−0.14 (8)	−0.14 (8)		
P_{22-}	0.25 (7)	0.24 (7)		
P_{31+}	−0.06 (6)	−0.06 (6)		
P_{31-}	0.21 (7)	0.20 (7)		

Table VI (Continued)

	refinement			
	I	II	III	IV
P_{33+}	0.58 (9)	0.61 (8)		
P_{33-}	−0.12 (9)	−0.11 (8)		
P_{40}	0.11 (8)	0.12 (7)		
P_{42+}	0.05 (7)	0.05 (7)		
P_{42-}	0.07 (8)	0.07 (8)		
P_{44+}	−0.14 (9)	−0.13 (8)		
P_{44-}	−0.17 (9)	−0.16 (8)		
C(4)B				
K	1.03 (1)	1.02 (1)		
$K'\zeta$	2.45 (2)	2.44 (2)		
P_v	4.21 (19)	4.19 (19)		
P_{11+}	0.07 (11)	0.07 (10)		
P_{11-}	−0.03 (11)	−0.02 (10)		
P_{20}	−0.34 (7)	−0.33 (7)		
P_{22+}	0.06 (8)	0.05 (8)		
P_{22-}	−0.07 (8)	−0.05 (8)		
P_{31+}	−0.14 (7)	−0.15 (7)		
P_{31-}	−0.05 (8)	−0.06 (7)		
P_{33+}	−0.47 (10)	−0.47 (9)		
P_{33-}	−0.30 (9)	−0.29 (9)		
P_{40}	0.16 (7)	0.15 (7)		
P_{42+}	0.00 (8)	−0.01 (8)		
P_{42-}	0.18 (8)	0.17 (8)		
P_{44+}	−0.01 (9)	−0.01 (9)		
P_{44-}	0.26 (9)	0.27 (9)		
C(5)B				
K	1.03 (1)	1.02 (1)		
$K'\zeta$	2.45 (2)	2.44 (2)		
P_v	4.19 (19)	4.19 (18)		
P_{11+}	0.22 (10)	0.22 (9)		
P_{11-}	0.06 (10)	0.07 (9)		
P_{20}	−0.17 (6)	−0.18 (6)		
P_{22+}	−0.33 (8)	−0.33 (8)		
P_{22-}	0.17 (8)	0.16 (7)		
P_{31+}	−0.14 (6)	−0.15 (6)		
P_{31-}	0.11 (7)	0.11 (6)		
P_{33+}	0.35 (9)	0.35 (8)		
P_{33-}	0.20 (9)	0.18 (9)		
P_{40}	0.05 (7)	0.07 (7)		
P_{42+}	−0.08 (7)	−0.08 (7)		
P_{42-}	−0.17 (8)	−0.17 (7)		
P_{44+}	0.33 (9)	0.32 (8)		
P_{44-}	−0.19 (9)	−0.18 (8)		
B				
K	1.18 (6)	1.16 (5)	1.15 (5)	1.09 (4)
$K'\zeta$	1.62 (5)	1.69 (6)	1.79 (6)	1.90 (5)
P_v	1.81 (30)	2.00 (29)	2.13 (30)	2.55 (26)
P_{11+}	−0.07 (17)	−0.08 (15)	−0.26 (11)	−0.23 (9)
P_{10}	−0.48 (16)	−0.43 (14)	−0.18 (10)	−0.24 (9)
P_{20}	−0.02 (12)	−0.04 (11)	0.16 (8)	0.09 (8)
P_{21+}	−0.18 (10)	−0.13 (8)	−0.20 (7)	−0.18 (6)
P_{22+}	0.01 (11)	0.02 (10)	0.10 (8)	0.10 (7)

	refinement			
	I	II	III	IV
P_{30}	−0.32 (18)	−0.36 (17)	−0.45 (14)	−0.46 (11)
P_{31+}	0.30 (12)	0.30 (11)	0.29 (9)	0.28 (7)
P_{32+}	0.22 (12)	0.19 (11)	0.29 (8)	0.25 (7)
P_{33+}	−0.82 (19)	−0.73 (15)	−0.57 (13)	−0.50 (10)
P_{40}	0.64 (22)	0.52 (18)	0.33 (14)	0.23 (11)
P_{41+}	−0.06 (9)	−0.06 (9)	−0.03 (7)	−0.04 (6)
P_{42+}	0.16 (14)	0.15 (13)	0.09 (9)	0.07 (8)
P_{43+}	−0.49 (18)	−0.46 (17)	−0.24 (13)	−0.29 (11)
P_{44+}	0.20 (15)	0.17 (13)	0.15 (10)	0.15 (8)
H(1)				
K	0.97 (4)	0.97 (4)	0.99 (4)	1.01 (3)
$K'\zeta$	1.58 (8)	1.60 (8)	1.63 (9)	1.77 (11)
P_v	1.19 (15)	1.16 (15)	1.13 (13)	1.04 (12)
P_{11+}	0.47 (13)	0.44 (12)	0.26 (19)	0.20 (6)
H(2)				
K	0.97 (4)	0.97 (4)	0.99 (4)	1.01 (3)
$K'\zeta$	1.58 (8)	1.60 (8)	1.63 (9)	1.77 (11)
P_v	1.02 (14)	0.99 (14)	0.97 (12)	0.88 (12)
P_{11+}	0.37 (12)	0.32 (11)	0.30 (18)	0.20 (6)
H(3)A				
K	0.97 (4)	0.97 (4)	0.99 (4)	1.01 (3)
$K'\zeta$	1.58 (8)	1.60 (8)	1.63 (9)	1.77 (11)
P_v	0.78 (12)	0.76 (12)	0.81 (9)	0.78 (9)
P_{11+}	0.27 (10)	0.26 (10)	0.47 (15)	0.19 (4)
H(4)A				
K	0.97 (4)	0.97 (4)	0.99 (4)	1.01 (3)
$K'\zeta$	1.58 (8)	1.60 (8)	1.63 (9)	1.77 (11)
P_v	0.93 (12)	0.92 (12)	0.82 (9)	0.92 (9)
P_{11+}	0.22 (10)	0.21 (10)	0.14 (13)	0.05 (5)
H(5)A				
K	0.97 (4)	0.97 (4)	0.99 (4)	1.01 (3)
$K'\zeta$	1.58 (8)	1.60 (8)	1.63 (9)	1.77 (11)
P_v	0.89 (12)	0.91 (12)	0.87 (9)	0.91 (8)
P_{11+}	0.32 (11)	0.34 (12)	0.28 (15)	0.20 (3)
H(3)B				
K	0.97 (4)	0.97 (4)		
$K'\zeta$	1.58 (8)	1.60 (8)		
P_v	0.72 (12)	0.71 (12)		
P_{11+}	0.39 (12)	0.37 (12)		
H(4)B				
K	0.97 (4)	0.97 (4)		
$K'\zeta$	1.58 (8)	1.60 (8)		
P_v	0.95 (13)	0.93 (13)		
P_{11+}	0.31 (12)	0.27 (13)		
H(5)B				
K	0.97 (4)	0.97 (4)		
$K'\zeta$	1.58 (8)	1.60 (8)		
P_v	0.98 (12)	0.98 (13)		
P_{11+}	0.30 (10)	0.31 (11)		

No refinement of isolated 4s electrons was attempted, due to the difficulty of determining the population of this diffuse orbital that peaks near the ligands; moreover, its contribution is partially taken into account by P_v.

In all the multipole refinements observations were weighted by $w = 1/\sigma^2(F_o^2)$; reflections with $I_{obsd} < 3\sigma(I_{obsd})$ were not included in the refinements. Final R factors are given in Table II. Multipole populations from refinements I–IV are given in Table VI.

The asymmetry in the electron density distribution around the Ni atom is evident in the negative population of the P_{44+} hexadecapole (−0.22, $y_{44+} = N \sin^4 \vartheta \cos 4\varphi$); in the equatorial plane ($\vartheta = 90°$) the function $P_{44+}y$ (with $P_{44+} < 0$) has minima for $\varphi = 0$, 90, 180, and 270° (the x and y axis directions) and maxima for $\varphi = 45$, 135, 225, and 315°; the Ni P_{44+} absolute value is slightly lower than the one found for Ni^{II} in nickel porphyrin[4] (−0.29), for Fe^{II} in iron phthalocyanine[9] (−0.28; −0.32), or for Co^{II} in CoTPP[10] (−0.26), indicating a lower distortion from a spherical density; the P_{20} population parameter ($y_{20} = N(3\cos^2\vartheta - 1)$) is positive (+0.25 to +0.26), indicating more than average occupancy in the z direction.

In D_{4h} the population parameters P_{lm} are related to the occupancies P_i of the $b_{1g}(d_{x^2-y^2})$, $a_{1g}(d_{z^2})$, $b_{2g}(d_{xy})$, and $e_g(d_{xz}, d_{yz})$ molecular orbitals by the relations

$$P_1(b_{1g}) = \tfrac{1}{5}P_{00} - 1.040P_{20} + 0.232P_{40} + 1.570P_{44+}$$

$$P_2(a_{1g}) = \tfrac{1}{5}P_{00} + 1.039P_{20} + 1.396P_{40}$$

$$P_3(b_{2g}) = \tfrac{1}{5}P_{00} - 1.040P_{20} + 0.232P_{40} - 1.570P_{44+}$$

$$P_4(e_g) = \tfrac{2}{5}P_{00} + 1.040P_{20} - 1.862P_{40}$$

With the values found in the multipole refinement imposing upon the Ni atom exactly the D_{4h} symmetry ($P_{00} = 9.28$ (2), $P_{20} = 0.25$ (2), $P_{40} = 0.05$ (2), and $P_{44+} = -0.22$ (1)), the following values are obtained for the occupancies: $P_1(b_{1g}, x^2 - y^2) = 1.26$ (13.6%);

Table VII. Atomic Charges (in e)

	spherical[a] or radial refinement	spherical harm. free, refinement II	spherical harm. constrained, refinement IV	ab initio model 1	ab initio model 2	ab initio pyrazole[b,c]
Ni	+1.18	+0.70	+1.06	+1.18	+0.86	
N(1)A	−0.33	−0.40	−0.32	−0.15	−0.17	−0.13
N(2)A	−0.21	−0.36	−0.26	−0.19	−0.19	−0.30
N(1)B	−0.34	−0.30			−0.17	
N(2)B	−0.40	−0.45			−0.19	
C(3)A	+0.33	+0.19	+0.03	+0.05	+0.06	+0.05
H(3)A		+0.24	+0.22	+0.11	+0.11	+0.11
C(4)A	−0.47	−0.30	−0.24	−0.08	−0.09	−0.19
H(4)A		+0.08	+0.08	+0.12	+0.11	+0.11
C(5)A	+0.38	0.00	−0.13	+0.09	+0.09	−0.03
H(5)A		+0.09	+0.09	+0.15	+0.14	+0.11
C(3)B	+0.23	0.00			+0.05	
H(3)B		+0.29			+0.11	
C(4)B	−0.13	−0.19			−0.09	
H(4)B		+0.07			+0.11	
C(5)B	+0.13	−0.19			+0.08	
H(5)B		+0.02			+0.14	
B	+0.63	+1.00	+0.45	+0.06	+0.26	
H(1)	−0.41	−0.16	−0.04	−0.08	−0.08	
H(2)	−0.02	+0.03	+0.12	−0.13	−0.10	
H(3)				−0.13		

[a] In the spherical refinement or radial refinement the atomic valence electrons are projected into a rigid spherical valence shell centered at the nucleus, described by a radial parameter K (see the major information: Becker, P., Ed. *Electron and Magnetization Densities in Molecules and Crystals*; Plenum: New York, 1980; p 464). We have found that, in this radial refinement, the atomic charge of an atom binding an hydrogen atom is not well-defined, depending greatly on the refinement condition, so it is better to define a total charge for the two atoms. [b] Reference 27. [c] The correspondence between the atomic numbering schemes of pyrazole and pyrazolylborate is questionable; we have chosen as N(2) the pyrazole nitrogen atom bearing the hydrogen atom.

$P_2(a_{1g}, z^2) = 2.19$ (23.6%); $P_3(b_{2g}, xy) = 1.95$ (21.0%); $P_4(e_g, xz, yz) = 3.88$ (41.8%).

It is clear that the occupancies obtained from the X-ray data differ from the populations expected for an isolated spherical Ni^{II} atom ($d_{x^2-y^2}$, 1.6 (20%); d_{z^2}, 1.6 (20%); d_{xy}, 1.6 (20%); d_{xz},d_{yz}, 3.2 (40%)) for a total of 8 electrons; in particular , the population of $d_{x^2-y^2}$ is lowered a fair amount while that of d_{z^2} is slightly increased.

The ζ value for the Ni atom, corresponding to radial dependence $R_l = r^4 \exp(-\zeta r)$, is found here to be 6.1 au^{-1}; a recent value for the same atom in (5,10,15,20-tetramethylporphyrinato)nickel(II)[4] is 8.358 au^{-1}, slightly higher than our value but very near the theoretical value for the isolated atom, 8.35, reported by Clementi and Raimondi.[24] We have obtained a more expanded nickel atom, i.e. K (0.97 against 1.00) and K' parameters smaller than those of ref 4. Although this may be related to the higher atomic charge of nickel in ref 4, any interpretation of the possible significance requires analysis of other similar compounds.

Some refinements were carried out with the K and K' radial parameters constrained to be equal for atoms related by $2/m$ molecular symmetry. We did not obtain any improvement of fit probably because the pyrazolyl ring itself possesses a mirror plane and such freedom is not necessary.

The multipole P_{lm} parameters, obtained in multipole refinement I, were used to produce "multipole model maps" according to

$$\rho_{\text{model}}(\mathbf{r}) = \frac{2}{V}\sum(F_{\text{calcd}}(\text{multipole model}) - F_{\text{calcd}}(\text{spherical atom}))\exp(2\pi i\mathbf{h}\cdot\mathbf{r})$$

These model electron density maps are virtually free from experimental random noise, because the parameters P_{lm} have undergone a least-squares process producing a "filtered" deformation map. All the reflections, even if weak and below the experimental cutoff, were used; i.e., the whole contribution to the ΔF series was included. This is particularly related to the weak high-angle reflections, where the contribution of valence electrons is predominant, especially for 3d orbitals of the Ni atom. In Figures 6–9 the corresponding model maps are presented; now the peaks around the Ni atom are clearly visible, condensed along the bisectrix of the x and y axes in accordance with the negative P_{44+} hexadecapole and indicating an accumulation upon the bond in the d_{xy} orbital. Figure 7 shows the deformation model map in the xz plane: there is an electron accumulation along the z direction in accordance with the positive P_{20} multipole parameter.

In the square-planar complexes of iron(II)phthalocyanine, $Fe^{III}(TPP)OCH_3$, or $Co^{II}(TPP)$ there is an evident electron deficiency in the z direction. This is explained by the lower number of d electrons with respect to that in Ni^{II}; in fact, also in the nickel compound of ref 4 an electron accumulaton in the z direction was found.

Residual density maps (observed density minus aspherical model density) calculated at the end of multipole refinements are essentially featureless, showing peaks ≤ 0.25 e/Å^3 positioned just where atoms are present; the maximum peak is present at the Ni atom position (this occurrence was already discussed before).

D. Atomic Charges: Experimental vs. ab Initio Results. In order to achieve some information on atomic charges with an independent method, we have performed ab initio computation on the model molecular ions

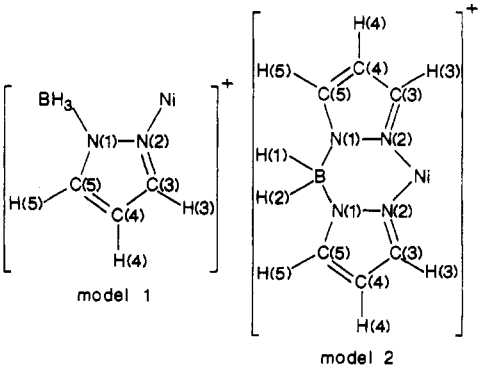

Only one (model 1) or two (model 2) pyrazolyl rings were introduced, to reduce computing time. The program used was GAUSSIAN 80;[25] it employs Gaussian basis sets of functions arranged

(24) Clementi, E.; Raimondi, D. L. *J. Chem. Phys.* **1963**, *38*, 2686–2689.

(25) GAUSSIAN 80, an "ab initio" MO program: Binkley, J. S.; Whiteside, R. A.; Krishnam, R.; Seeger, R.; De Frees, D. J.; Schlegel, H. B.; Topiol, S.; Kahn, L. R.; Pople, J. A. *Quantum Chemistry Program Exchange, Indiana University*, 1980, Program 446 (VAX version).

Table VIII. Ab Initio Bond Order Values, Peak Heights (e/Å^3), and Distances (Å) in $[H_2B(C_3N_2H_3)_2]_2Ni^{II}$

	ab initio[a]	multipolar[b]	exptl[c]	dist[d]
N(1)–N(2)	0.35	0.40	0.46	1.3555
N(1)–C(5)	0.46	0.41	0.40	1.3425
N(2)–C(3)	0.44	0.41	0.42	1.3430
C(3)–C(4)	0.52	0.60	0.55	1.3960
C(4)–C(5)	0.50	0.44	0.54	1.3920

[a] Ab initio bond order values between indicated atoms from model 2 (values from model 1 are indeed very similar). [b] Peak height in the middle of the indicated atoms after multipolar analysis (refinement IV, map in Figure 9). [c] As in *b* but from experimental maps in Figure 5, as a mean of rings A and B. [d] Distance as a mean of rings A and B at 150 K.

into shells in a contracted manner. The extended basis sets used here consist of the (12,7,5) Gaussian basis set of nickel reported in ref 26 and augmented with a 4s function with exponent 0.2 and with a 3d function also with exponent 0.2; this basis set was then contracted to [6221/421/41]. The radial wave functions on C, N, and H atoms are taken from the internally stored STO–3G bases with $S = P$ constraints (2s and 2p functions with the same exponents).

The atomic charges obtained with this method are reported in Table VII together with those experimentally obtained with X-ray data refinement methods. Generally there is a good qualitative agreement among various refinement methods and various ab initio methods, so following Preston and Kaufman[27] we may say that the heteroatoms (N(1) and N(2)) draw electron density, that C(3) is slightly electron deficient and that the other carbon atoms have a slight excess of electron density. Likewise, the H atoms at the C atoms are σ-electron donors, producing electron-deficient (0.1–0.2 e) hydrogen atoms. Moreover, the C(4) atom is predicted to be the most negative carbon atom in the ring because it is far away from the two N atoms.

The Ni atomic charge is predicted to be $\simeq$+1.0 e, and Ni does not bear a dipositive charge as would be implicit in a ionic formula. Coppens et al.[5] in the [*N*,*N*′-bis(2-aminoethyl)malonodiamidato]nickel(II) trihydrate complex have found for the Ni atom a positive charge of about +0.5 e also using accurate X-ray diffraction data.

The high atomic charge (+0.45 e) at the B atom calls for some comment as well. This B atom is bonded to highly electronegative N atoms, and a high charge must be expected; moreover, the only known example of an $X - X$ electron density map regarding a B–N bond was reported by Hseu[28] for 1,1,4,4-tetramethyl-1,4-diaza-2,5-diboracyclohexane, an interesting compound containing the cyclohexane-like ring $\overline{NBCNBC}$. The $X - X$ map suggests a positive B atom and shows a peak (of height 0.12 e/Å^3) exactly in the middle of the B–N bond. Our situation is something different indeed, because the B–N bonding electrons are shifted toward the N atoms (Figures 2, 5, 8, and 9), thus rendering the B atom highly charged.

A more intriguing examination of ab initio and experimental electron density is to compare the bond order as obtained by the theoretical method and experimental peak heights as shown in Table VIII. The qualitative agreement is good again; in particular the pyrazolyl ring shows a quasi mirror plane passing through the C(4) atom and the middle of the N(1)–N(2) bond: C(3)–C(4) $\simeq$ C(4)–C(5), N(1)–C(5) $\simeq$ N(2)–C(3), and the peak heights are roughly equal. Moreover, the C(3)–C(4) bond shows the highest electron density as well as the highest bond-order character.

Acknowledgment. We are grateful to Prof. G. Paolucci for supplying a sample of the compound. This investigation was financially supported by the MPI and in part by the CNR, Rome, Italy (Grant Nos. 84.00660.03 and 85.01466.03). We are very indebted to Prof. P. Coppens and Dr. R. Ortega of the State University of New York at Buffalo for supplying the MOLLY 81 program, to Dr. B. Rees of the CNRS, University of Strasbourg, and Dr. N. K. Hansen of the Hahn-Meitner Institut, West Berlin, West Germany, for helpful discussions.

Registry No. $[H_2B(C_3H_2N_3)_2]_2Ni^{II}$, 18131-13-0.

Supplementary Material Available: Table S1, listing anisotropic thermal parameters from high-order refinement, and Table S2, listing isotropic thermal parameters for hydrogen atoms (1 page); tables of observed and calculated structure factors at 150 and 183 K (61 pages). Ordering information is given on any current masthead page.

(26) Roos, B.; Veillard, A.; Vinot, G. *Theor. Chim. Acta* **1971**, *20*, 1–11.
(27) Preston, H. J. T.; Kaufman, J. J. *Int. J. Quantum Chem. Symp.* **1973**, *No. 7*, 207–215.
(28) Hseu, T. H. *J. Mol. Struct. No.* **1979**, *53*, 121–127.